The Meteoritical Society

Meteoritics & Planetary Science 51, Nr 2, 261–275 (2016)
doi: 10.1111/maps.12581

Space weathering of silicates simulated by successive laser irradiation: In situ reflectance measurements of Fo_{90}, Fo_{99+}, and SiO_2

M. J. LOEFFLER[1*], C. A. DUKES[2], R. CHRISTOFFERSEN[3], and R. A. BARAGIOLA[2†]

[1]NASA Goddard Space Flight Center, Greenbelt, Maryland 20771, USA
[2]University of Virginia, Laboratory for Astrophysics and Surface Physics (LASP), Charlottesville, Virginia 22904, USA
[3]Jacobs, NASA Johnson Space Center, Mail Code XI3, Houston, Texas 77058, USA
[†]Deceased
[*]Corresponding author. E-mail: mark.loeffler@nasa.gov

(Received 16 June 2015; revision accepted 19 October 2015)

Abstract–Pulsed-laser irradiation causes the visible-near-infrared spectral slope of olivine (Fo_{90} and Fo_{99+}) and SiO_2 to increase (redden), while the olivine samples darken and the SiO_2 samples brighten slightly. XPS analysis shows that irradiation of Fo_{90} produces metallic Fe. Analytical SEM and TEM measurements confirm that reddening in the Fo_{90} olivine samples correlates with the production of "nanophase" metallic Fe ($npFe^0$) grains, 20–50 nm in size. The reddening observed in the SiO_2 sample is consistent with the formation of SiO or other SiO_x species that absorb in the visible. The weak spectral brightening induced by laser irradiation of SiO_2 is consistent with a change in surface topography of the sample. The darkening observed in the olivine samples is likely caused by the formation of larger $npFe^0$ particles, such as the 100–400 nm diameter $npFe^0$ identified during our TEM analysis of Fo_{90} samples. The Fo_{90} reflectance spectra are qualitatively similar to those in previous experiments suggesting that in all cases formation of $npFe^0$ is causing the spectral alteration. Finally, we find that the accumulation of successive laser pulses cause continued sample darkening in the Vis-NIR, which suggests that repeated surface impacts are an efficient way to darken airless body surfaces.

INTRODUCTION

Airless planetary bodies are constantly being bombarded with multiple types of radiation and hypervelocity meteorite impacts, such that their surface regoliths undergo a diversity of physical, chemical, and optical changes known as space weathering (Hapke 2001; Clark et al. 2002; Chapman 2004). Identifying the "markers" that indicate a space weathered regolith is important not only for understanding how the surface evolves over time but also for accurately determining the composition of the intrinsic surface by remote sensing techniques. One of the most commonly utilized techniques for characterizing surfaces of airless bodies is optical reflectance spectroscopy. Ideally the remotely sensed reflectance spectrum of a surface can be compared with a relevant laboratory spectrum of extraterrestrial or analog material to yield information on the surface's composition, mineralogy, and origin.

For the case of planetary surfaces with an abundance of mafic minerals, such as S-type asteroids and the Moon, there are key indicators for surface alteration via radiation or meteorite impact. Compared to unweathered minerals of assumed similar composition, the near-infrared (~0.6–2.5 μm) reflectance spectra is usually more sloped (redder), lower in reflectance (darker), and contains weaker absorption features (Gaffey 2010).

Laboratory studies have been generally successful in reproducing the space weathering characteristics seen in lunar and S-type asteroid spectra by focusing on the changes caused by energetic ions and micrometeorite hypervelocity impacts. Using keV protons as a solar wind analog, early studies (Nash 1967; Hapke 1973) showed that irradiation caused the reflectance spectrum of the analog and returned lunar samples to evolve toward the in situ lunar soil spectra, becoming darker, redder, and having attenuated absorptions. Through more detailed studies (see Hapke [2001] for a review),

Hapke was able to show that to create spectral changes consistent with space weathering, the sample needed to contain Fe. The effect was enhanced when using a fine-grained, powder sample (Pieters et al. 1993; Hapke 2001). The chemical reduction of Fe found in both ion irradiated and natural lunar soils (Yin et al. 1975; Housley and Grant 1977) seemed to support the assertion that solar wind chemical reduction of Fe could be causing spectral results of weathering. Subsequent analytical transmission electron microscope (TEM) observations supported the hypothesis that the Fe was chemically reduced and found that most of it was in the form of 5–100 nm diameter metallic Fe spherules residing in altered rims on lunar regolith grains, as well as in the glassy portions of glass-welded aggregates known as agglutinates (Keller and McKay 1993, 1994, 1997). For the solar wind specifically, laboratory studies have since shown that direct keV ion irradiation can chemically reduce Fe on the surfaces of Fe-bearing minerals such as olivine (Dukes et al. 1999; Davoisne et al. 2008; Loeffler et al. 2009), and that this reduction correlates with the observed spectral reddening (Loeffler et al. 2009). In addition, Noble et al. (2007) showed that simply adding fine-grained (<10 nm) metallic Fe to an nonabsorbing silicate gel caused reddening of the sample spectrum.

Early simulations of meteorite impacts focused on vitrification of regolith grains, because glass formation appeared to alter the reflectance spectra of various types of samples (Nash and Conel 1973; Hapke et al. 1975). However, there is still some debate on why darkening and attenuation of absorption bands were found in some experiments (Adams and McCord 1971; Nash and Conel 1973) and not in others (Hapke et al. 1975); see Hapke (2001) for more discussion. Other experiments that investigated the synergistic effects of heating and comminution during impacts found little change in reflectance with comminution alone, but qualitative reddening and darkening with repeated comminution-melting cycles (Clark and Fanale 1992). However, these results have also been questioned (Hapke 2001).

More recent attempts to simulate the conditions in micrometeorite impacts have used pulsed-laser beams with instantaneous power densities (W cm^{-2}) similar to those of typical impacts by micron-sized meteorites (Moroz et al. 1996; Sasaki et al. 2001; Brunetto et al. 2006a; Loeffler et al. 2008; Noble et al. 2011). These studies have shown laser irradiation, like ion irradiation, can cause the near-infrared reflectance spectra of mafic minerals to redden, and may cause significant darkening as well. These spectral changes are consistent with those in weathered lunar samples, which are known to contain $npFe^0$. However, although the SEM results of Moroz et al. (1996) showed that all laser-irradiated samples contained glassy deposits and that the olivine samples contained Fe-rich regions, the spatial resolution of their microprobe analysis was not sufficient for them to determine whether any of these regions contained reduced "nanophase" Fe ($npFe^0$). Later, Sasaki et al. (2001, 2003) used transmission electron microscopy and electron spin resonance (ESR) to show that the Fe-rich regions formed in laser-irradiated olivine and pyroxene samples contained reduced $npFe^0$, supporting the hypothesis that the observed optical changes are driven by the presence of reduced $npFe^0$ particles. Most recently, Brunetto et al. (2006a) suggested that, besides formation of $npFe^0$, structural modification induced by the pulsed laser may be important, as the rapid melting of the sample may not only change the phase of the silicates but could also induce irregular structures that may change the scattering properties of the minerals.

These previous laser irradiation studies have clearly shown that the laser can generate both melt and vaporized material on mineral and rock surfaces creating a variety of structures which, given the presence of Fe in the target material, can contain $npFe^0$ particles. However, there have been no experiments explicitly showing that the observed spectral changes correlate directly with the formation of metallic Fe, because none of the previous studies employed a microanalytical technique that could monitor metallic Fe content during laser irradiation. In addition, although previous investigations studied different mafic minerals, none varied the Fe content within the same mineralogical family, a strategy which could clarify the role structural modification plays in the alteration of reflectance spectra. In this work, we have investigated the role that Fe content plays when a key silicate, olivine, is irradiated with a pulsed laser operated to simulate conditions during micrometeorite impact. Besides being directly applicable to previous laser irradiation studies mentioned above, olivine is a major component in chondritic meteorites and has been identified in numerous asteroids (Sanchez et al. 2014), and is also a significant lunar mineral (Gaffey et al. 1993; Hapke 2001; Clark et al. 2002). This article is a companion work to our previous studies on the spectral and chemical effects of vapor redeposition and ion irradiation (Loeffler et al. 2008, 2009). The unique aspect of our approach has been that, in addition to measuring the reflectance spectra of our sample, we can also monitor the chemical evolution of our sample using X-ray photoelectron spectroscopy (XPS). This has allowed us to show the correlation between spectral reddening and chemical reduction of Fe in ion irradiated Fo_{90} San Carlos olivine (Loeffler et al. 2009).

In the current experiments, we used a 193 nm ns-pulsed laser to irradiate, under ultrahigh vacuum, flat-sectioned surfaces of single-crystals and powders of Fo_{90} San Carlos olivine, as well as powders of nearly pure synthetic forsterite and SiO_2. During pulsed-laser irradiation, we monitored both the near-infrared reflectance spectra and the surface chemical composition of our samples in situ, e.g., without exposing the samples to the atmosphere. In addition to the in situ measurements, we also performed ex situ measurements using ultraviolet-visible reflectance spectroscopy, and scanning and transmission electron microscopies on select samples to measure changes in surface structure, including Fe nano-particle production.

EXPERIMENTAL METHODS

Sample Preparation and In Situ Analysis

The majority of the experiments reported here were on powders sieved to a 45–125 μm size fraction and pressed into an aluminum ring to make a ~10 mm diameter by ~2 mm thick pellet disk. The slightly larger grain size in our pellets, compared to our previous work (<45 μm; Loeffler et al. 2008, 2009), was needed to prevent the sample from disintegrating during laser irradiation. The pellets were prepared from natural San Carlos olivine (Fo_{90}; $Mg_{1.8}Fe_{0.2}SiO_4$; Penn Minerals), synthetic SiO_2 (99.99%; Alfa Aesar) and synthetic forsterite (Fo_{99+}; Reade Advanced Materials). The synthetic forsterite is listed as containing 0.02 wt% Fe_2O_3 as an impurity ($\cong Fo_{99.9}$), along with Al_2O_3 (0.03), TiO_2 (0.09), Na_2O (0.11), CaO (0.22), and K_2O (0.12). In addition to the pressed pellets, we also performed experiments on flat unpolished sections of San Carlos olivine single-crystals several mm in size (Arizona Gems and Crystals).

After preparation, the samples were mounted on a copper holder and transferred into an oil-free ion-pumped ultrahigh vacuum (UHV) chamber with a base pressure of $5–10 \times 10^{-10}$ Torr (see Loeffler et al. 2009). Surface analyses of the samples were performed before, during, and after irradiation using X-ray photoelectron spectroscopy (XPS) and near-infrared reflectance (NIR) spectroscopy. More details on sample preparation and our in situ analysis methods are given in Loeffler et al. (2009).

Laser Irradiation

A typical approach to simulating micrometeorite impacts employs high-energy pulses from a nanosecond laser (Yamada et al. 1999; Sasaki et al. 2001; Brunetto et al. 2006a). This technique has the advantage, compared to the more traditional approach of accelerating dust particles from a dust accelerator (Cintala 1992), of uniform irradiation over macroscopic areas with a relatively high-energy flux. Analysis of laser-irradiated samples shows that this method successfully produces spectral changes consistent with micrometeorite impact (Sasaki et al. 2001). Besides the experimental evidence, the justification for using ns-pulsed lasers to mimic dust impacts has also been made by comparing the composition of thermoionic plasma emitted from samples that were impacted by accelerated dust and laser beams (Kissel and Krueger 1987), normalized to the deposited power density (W cm^{-2}). Kissel and Krueger (1987) showed that, above the laser ablation threshold, similar ejected ion mass spectra and absolute yields are obtained when the power density of the laser beam is ~100 times lower than that for dust impact, as a result of the different efficiency of conversion of impact energy to temperature (Sugita et al. 2003). With this in mind, we estimate that the UV laser pulses used in our experiments (~10^8 W cm^{-2}) are roughly equivalent to a 1–20 μm particle (2 g cm^{-3}) traveling ~10–15 km s^{-1}. On impact, this is equivalent to a power density of 10^{10} W cm^{-2} assuming that all the energy is deposited over an area given by the cross section of the dust particle, and a depth of 3 particle diameters. We note that even micrometeorite impacts as slow as 0.05 km s^{-1} can produce a thermionic plasma and, hence, vaporization (Smith and Adams 1973).

In the experiments reported here, we irradiated our samples at normal incidence with a GAM ArF excimer laser that emits 10 ns pulses of 193 nm light at 1 Hz. During irradiation, the normal of the sample surface was horizontal. The laser beam entered the analysis chamber through a quartz-fused silica window and was imaged to a 0.5 mm^2 spot on the sample surface; each pulse had an energy fluence of 1 J cm^{-2}. The beam was rastered uniformly across the sample with mirrors actuated by a motion control system synchronized to the laser. During each raster sequence, the sample was monitored to ensure that only the pellet material (not the Al ring) was irradiated. Finally, we note that in the text when we describe one laser pulse, we mean that the laser has been rastered across the sample one time, so that each region of the analyzed area has been irradiated once.

Ex Situ Analysis

After irradiation and in situ analysis, selected samples were subsequently analyzed by additional methods after removal from the UHV irradiation chamber. These additional ex situ analyses included: ultraviolet-visible spectroscopy, analytical field-emission scanning electron microscopy (FE-SEM) and analytical field-emission scanning transmission electron

microscopy (FE-STEM). For the ultraviolet-visible measurements, we used a FilmTek fiber optic spectrometer over the wavelength range of 250–600 nm, at a resolution of 0.2 nm. Light was incident normal to the sample's surface and reflected light was collected at 45 degrees. The reflectance spectrum was obtained by dividing the collected light from the sample by the reference, after subtraction of the dark spectrum, to yield the reflectance value: $R = (I_{sample} - I_{Dark})/(I_{reference} - I_{Dark})$. The reference sample was a Spectralon™ reflectance standard obtained from Labsphere. However, as the absolute reflectance values are not provided at the lower wavelengths, we do not consider our processed reflectance spectrum to be an absolute one. Given the minor difference between the phase angle in the UV and near-infrared reflectance measurements, lack of absolute standard in the UV etc., we are not surprised by the slight reflectance variation in the data we can see in SiO_2 and to a lesser extent, in the other two samples (compare Figs. 1, 2, and 5).

Following ex situ optical spectroscopy, field-emission scanning electron microscopy characterization was performed on selected samples utilizing a JEOL 7600F field-emission SEM, which can acquire secondary/backscattered electron images (SEI/BSE) and compositional element maps with a Thermo® energy-dispersive X-ray (EDX) spectrometer system. Regions of particular microstructural or compositional interest were then prepared for field-emission scanning transmission electron microscopy characterization by focused ion beam (FIB) lift-out sectioning using an FEI Quanta dual electron/ion beam milling instrument. FE-STEM characterization utilized a JEOL 2500SE FE-STEM with compositional element mapping capabilities provided by a Thermo® EDX compositional spectrum imaging system. X-ray counts for individual EDX spectra and element maps were converted to wt% element concentrations using the Cliff-Lorimer quantification technique, which is based on empirically determined k-factors (Cliff and Lorimer 1975).

RESULTS

Fluence Dependence of Near-Infrared Reflectance

Figure 1 shows the near-infrared reflectance (unpolarized) of the Fo_{90}-pressed pellet sample, measured in situ as a function of the accumulated number of individual 1 J cm^{-2} rastered laser scans. The Fo_{90} absolute reflectance spectrum (Fig. 1 top) shows the absorption features characteristic of polycrystalline olivine, due to electronic excitation of the outer 3d-electrons of Fe^{2+} (Burns 1993). The spectrum of the unirradiated sample is similar to spectra reported in

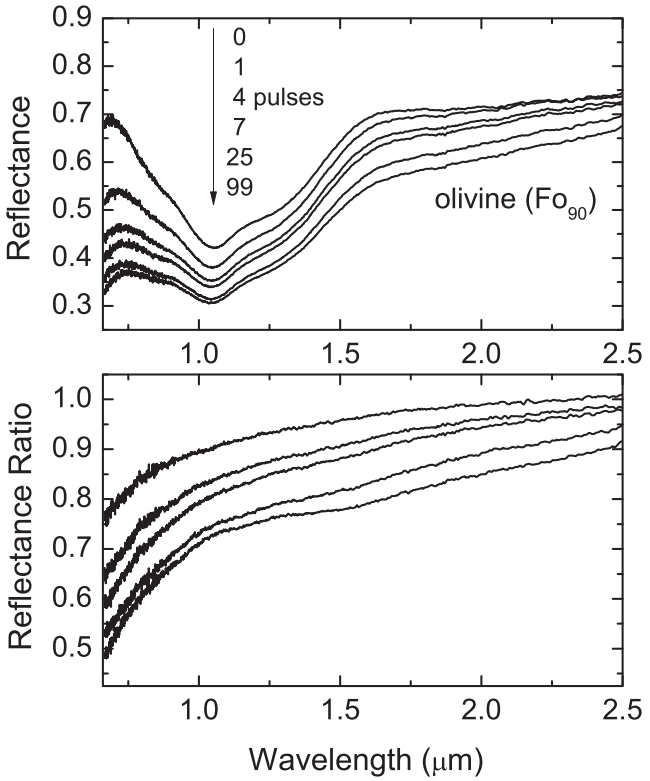

Fig. 1. Top) Absolute reflectance spectra of Fo_{90} powder after (from top to bottom at 700 nm): 0, 1, 4, 7, 25, and 99 laser pulses. Bottom) Reflectance of Fo_{90} powder divided by that from the unirradiated sample; the spectra (from top to bottom at 700 nm) correspond to 1, 4, 7, 25, and 99 laser pulses. One laser pulse represents ~10^8 W cm^{-2}.

previous studies on San Carlos olivine (Yamada et al. 1999; Sasaki et al. 2001; Brunetto et al. 2006a). The data in Fig. 1 show clear evidence that consecutive laser irradiations cause systematic changes in the Fo_{90} pellet sample: the spectral slope increases, the overall reflectance decreases, and 1 μm absorption band attenuates. To highlight the changes in the sample solely due to irradiation, we show the ratio of the spectra of the irradiated olivine sample to that of the unirradiated olivine sample (Fig. 1 bottom). Similar changes in spectral shape have been reported previously for various types of laser-processed olivine samples, including pulsed-laser deposits formed on powdered olivine substrates using olivine irradiation targets (Loeffler et al. 2008), direct laser ablation of olivine (Brunetto et al. 2006a), olivine impacted by high-energy (60–400 keV) ions (Strazzulla et al. 2005; Brunetto et al. 2006b), and low energy (4 keV) ions (Loeffler et al. 2009). As in our previous ion irradiation experiments (Loeffler et al. 2009), we find that there is no clear shift in the band center during irradiation.

To determine if pulsed-laser irradiation can alter the reflectance and composition of a non-Fe-bearing

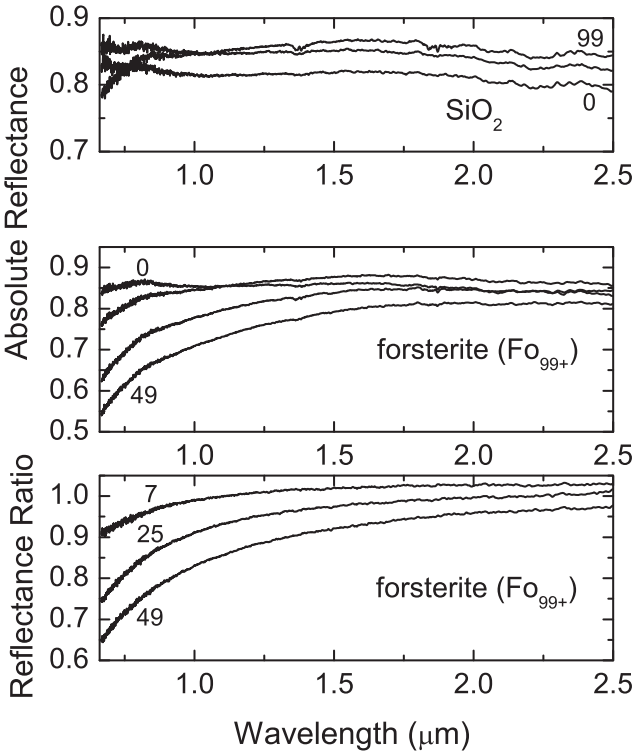

Fig. 2. Top) Absolute reflectance spectra of a SiO_2 powder after (from bottom to top at 2 μm): 0, 1 and 99 laser pulses. Middle) Absolute reflectance spectra of Fo_{99+} powder after (from top to bottom at 700 nm): 0, 7, 25, and 49 laser pulses. Bottom) Reflectance of Fo_{99+} powder divided by that from the unirradiated sample; the spectra (from top to bottom at 700 nm) correspond to 7, 25, and 49 laser pulses.

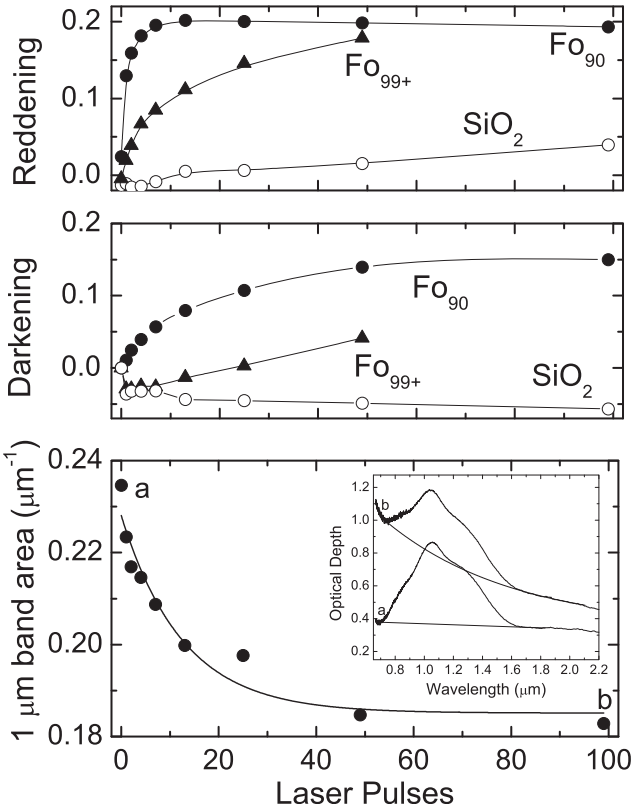

Fig. 3. Top) Reddening ($r = [R_{2.0\ \mu m} - R_{0.7\ \mu m}]/1.3$ μm), where R is the reflectance. Middle) darkening at 2 μm ($1 - R/R_o$) where R_o is the reflectance of the unirradiated sample. Bottom) Decrease in the 1 μm band area (circles) as a function of laser pulses for a Fo_{90} powder. Inset) Baseline fit of the olivine optical depth spectra (in $-\ln(R)$ units) used to measure the band area, before (a) and after (b) laser irradiation with 99 pulses.

mineral, we irradiated pressed pellets of both Fo_{99+} and SiO_2 powders. Figure 2 (top) shows the absolute reflectance spectrum of SiO_2 powder. The spectral changes induced by the laser are much less than what was observed in the Fo_{90}, yet the overall trend is clearly greater than our estimated experimental error (<1%). Figure 2 (middle) shows the absolute reflectance spectra of the Fo_{99+} powder during irradiation, while Fig. 2 (bottom) shows the ratio of the spectrum of the irradiated sample to that of the unirradiated sample. Although the synthetic forsterite has less than a tenth of the Fe as compared to our San Carlos sample, its spectral slope increases and, after the first laser pulse, overall reflectance decreases with increasing irradiation. These results are different from what we observed when we vapor deposited Fo_{99+} onto silicate powders, where only a low amount of reddening was observed (Loeffler et al. 2008).

To quantify the spectral changes observed in our three types of samples, we compare the changes in the spectral slope (reddening) in Fig. 3 (top). As previously (Loeffler et al. 2009), we define reddening as $r = (R_{2.0\ \mu m} - R_{0.7\ \mu m})/1.3$ μm, where 1.3 μm is the wavelength interval. For the Fo_{90} pellet sample, only one laser pulse is needed to bring it halfway to its most reddened value, achieved after 49 pulses. Fo_{99+} and SiO_2 redden in a more gradual fashion with laser fluence, and do not reach steady state within the time frame of our experiment. We note that although the laser causes the Fo_{99+} sample to redden less than the Fo_{90} sample initially, the Fo_{99+} sample continues to redden with laser irradiation and after 49 pulses the two samples are nearly equally reddened. The SiO_2 is actually slightly "blue" before irradiation, but reddens moderately as it is irradiated. By the time the fluence reaches 99 pulses, the reddening is still more than a factor of three less than what we observed for the other samples and does not appear to have reached a steady state.

In addition to reddening, data for sample darkening are shown in Fig. 3, with darkening parameterized as $1 - R/R_o$ at 2 μm, where R_o is reflectance of the unirradiated sample. The Fo_{90} pellet sample darkens

during irradiation and appears to reach a steady-state value of ~15% after 99 laser pulses. The Fo_{99+} and SiO_2 samples show a different behavior. After only one pulse, both samples appear to brighten slightly. The SiO_2 continues to slowly brighten throughout the irradiation up to a value of ~6%. However, after the initial brightening, additional irradiation does not change the Fo_{99+} sample's reflectance until after 13 pulses, where the sample darkens linearly up to the last set of pulses (49 pulses) to a value of 5%.

For the Fo_{90} sample, we quantified the area of the 1 μm absorption band by converting the spectrum to optical depth units, taking the natural logarithm of the reflectance, and subtracting a nonlinear baseline (Fig. 3 bottom). This method is the same as that used in our previous ion irradiation study on Fo_{90} (Loeffler et al. 2009). Figure 3 shows that, as the sample is irradiated, the area of the 1 μm absorption band decreases by 20% after 99 laser pulses. The slight decrease in the absorption band depth also is evident in the olivine ratio spectrum (Fig. 1 bottom, 99 pulse spectrum).

X-Ray Photoelectron Spectroscopy

During laser irradiation, changes in the surface chemical composition of the Fo_{90} and Fo_{99+} samples were monitored with XPS. We acquired initial survey spectra and also high-resolution spectra for chemical analysis of the main elements (O, C, Fe, Mg, and Si). The spectra were compared as follows. First, the spectra were all shifted to compensate for residual electrostatic charging, so that the peak position of Si-2p oxide was aligned; this shift was <0.5 eV. Next, the absolute binding energy scale was determined from the position of the C-1s peak for adventitious carbon in the initial spectra at 284.8 eV. The binding energies measurements for our samples are in good agreement with previously published values of olivine (Dukes et al. 1999), forsterite (Hochella and Brown 1988), fayalite (Schott and Berner 1983), and $Mg_{1.2}Fe_{0.8}SiO_4$ (Yin et al. 1971). The Fo_{99+} sample was found to contain detectable Fe, but the amount was so low that the chemical changes could not be easily followed.

For the Fo_{90} and Fo_{99+} samples, we did not observe significant changes in the O-1s (531.4 eV), Mg-2p (50.1 eV), or Si-2p (101.8 eV) photoelectron peaks resulting from laser irradiation. In particular, no formation of metallic Mg or elemental Si was detected, although the Mg-2p and Si-2p peaks did broaden slightly suggesting that some chemical reduction occurred. As the pellet samples were not prepared under vacuum conditions, they all showed initially some atmospheric contamination, evidenced by the presence of the C-1s adventitious carbon peak at 284.8 eV. After

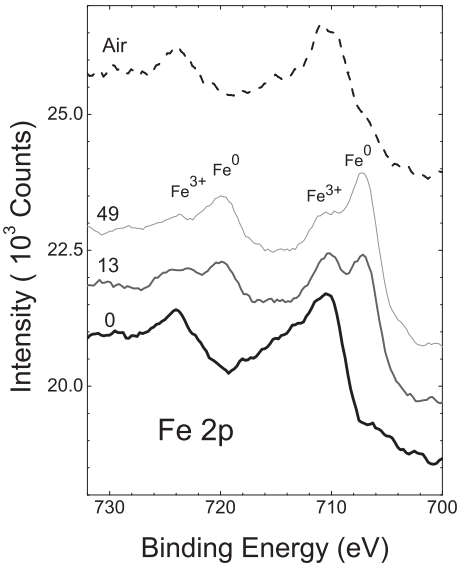

Fig. 4. X-ray photoelectron spectra of the Fe-2p region of a Fo_{90} powder during laser irradiation. The bottom three spectra are after (from bottom to top): 0, 13, and 49 pulses. The top spectrum (dashed) is after exposing the irradiated sample to atmosphere for 10 min.

1–2 laser pulses, the surface carbon signal decreased to the noise level of the instrument. In addition to the adventitious carbon peak, there appeared to be a second, minor, C-1s peak present at 283.8 eV that remained throughout the experiment indicating carbon intrinsic to the samples.

Besides the removal of carbon surface contaminants at low fluences, the only other major change observed was chemical reduction, apparent in the Fe-2p transition of the Fo_{90} sample (Fig. 4). The initial peak position of the Fe-2p band indicates that Fe is not in the form of Fe^{2+} (709.1 eV) expected for the bulk olivine sample, but rather as Fe^{3+} (711.4 eV) on the surface. These results are in agreement with previous experiments (Schott and Berner 1983; Dukes et al. 1999). Continued irradiation of the Fo_{90} olivine powder increasingly reduces the Fe on the surface to the metallic state (Fe^o, 706.7 eV), attaining a steady-state level of near 0.7 Fe^o/Fe represented by the 49 pulse spectrum. This value is similar to the steady-state value observed as a result of ion irradiation (Loeffler et al. 2009), but slightly lower than that of a laser-irradiated flat olivine section. We will return to this topic in the discussion section.

After laser irradiation and in situ analysis, we exposed the laser-irradiated Fo_{90} powder sample to atmosphere for ~10 min, and then reacquired the XPS and NIR spectra. The Fe on the surface of the olivine is nearly completely re-oxidized (top spectrum in Fig. 4), as determined by XPS, while the reflectance spectra is virtually unchanged (data not shown here), consistent

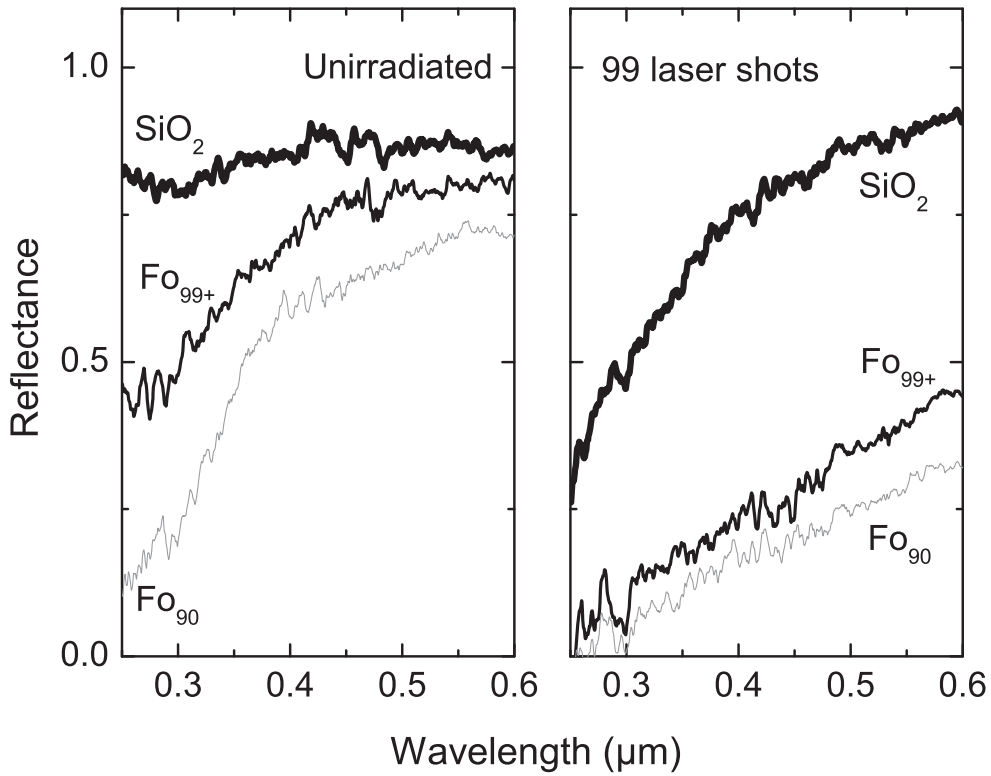

Fig. 5. Ex situ ultraviolet-visible reflectance spectra of mineral powders before (left panel) and after (right panel) laser irradiation.

with our previous work (Loeffler et al. 2009). This implies that the reoxidized layer, while thicker than the XPS sampling depth (~5–8 nm for our sample) (Seah and Dench 1979) is much thinner than the layer created by the laser.

Ex Situ UV Reflectance

We also measured the ultraviolet-visible reflectance of some of our samples before and after irradiation (Fig. 5). The left panel shows the sample reflectance before irradiation; it is clear that there is significant UV absorption in the reflectance spectrum of the Fo_{90} and Fo_{99+} samples, while the spectrum of SiO_2 is spectrally flat within error. The SiO_2 spectrum is consistent with previous studies (Philipp 1966). The absorption observed for the Fo_{90} sample is also expected, as it is derived from the relatively strong Fe oxide charge transfer band at 260 nm, an allowed transition for Fe^{2+}–O^{2-} in olivine (Hapke 2001). The absorption present in the Fo_{99+} spectrum is presumably due to the Fe impurities present the sample, which can exist as Fe^{2+} or Fe^{3+}, as the closest reported transition in the region for a completely iron-free sample is due to the band gap transition near ~150 nm (Nitsan and Shankland 1976). We note that previous studies have shown that even very low Fe/Mg ratios in synthetic forsterite can show observable absorption bands as both Fe cations absorb in this region (Shankland 1968; Nitsan and Shankland 1976; Balberg and Pinch 1978).

After irradiation with 99 laser pulses, all samples showed a decrease in reflectance in the ultraviolet. Surprisingly, the SiO_2, with no known absorption bands above ~120 nm and no metallic Fe present, shows a definite decrease in UV reflectance, which extends up to ~500 nm. The shape of the reflectance curves for the Fo_{90} and Fo_{99+} samples look fairly similar after irradiation. Both spectra lose their curvature below 400 nm and become linear, dropping in reflectance with decreasing wavelength. Examination of the slope for these two samples shows that between 300 and 400 nm the slope decreases by a factor of two for Fo_{99+} and a factor of 3.5 for Fo_{90}. This decrease in slope with irradiation is consistent with the observation by Hendrix and Vilas (2006), who found that the spectral slope in this region is also lower for weathered asteroids and lunar soil.

Analytical Field-Emission SEM and STEM

After 99 laser pulses, the Fo_{90} pressed-pellet powder sample was analyzed by FE-SEM and FE-STEM

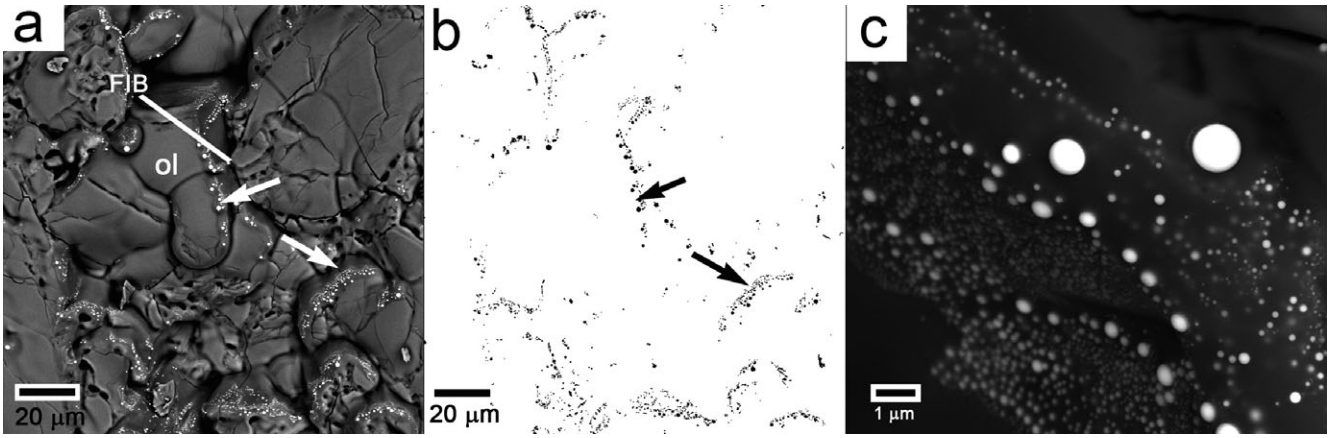

Fig. 6. FE-SEM images of the surface of the Fo_{90} powder pellet after 99 laser pulses. a) Low-magnification SEM backscattered electron (BSE) image showing areas with concentrations of nanophase metallic Fe grains (white speckles). Arrows indicate areas of particularly high concentrations of nanophase metallic Fe grains. The white line labeled FIB shows the transect across an olivine grain (ol) where a FIB section was extracted for FE-STEM analysis (Fig. 7). The olivine grain is bounded by depressions in the sample surface on its top and right sides. b) Same image area as (a) after use of contrast threshold processing to show distribution of nanophase metallic Fe grains as black dots and speckles. c) Higher magnification FE-SEM BSE image of concentrated area of nanophase metallic Fe grains (white dots and speckles).

methods. Figure 6 shows a representative region of the sample surface imaged by FE-SEM backscattered electron (BSE) imaging. Figure 6a shows areas (indicated by arrows) with locally high concentrations of submicrometer, spherule-shaped grains that were confirmed to be metallic Fe ($npFe^0$) based on subsequent FE-STEM characterization (see Fig. 7). The $npFe^0$ is hosted in laser-altered material concentrated within narrow gaps between grains and on the sloping sides of grains that border larger surface depressions. Averaged over the area of Fig. 6a, the $npFe^0$ modal percentage is approximately 0.5% based on the corresponding threshold-processed image in Fig. 6b. The average grain size of $npFe^0$ visible at the resolution of most BSE images is approximately 100 nm, but a broad size distribution is typical as shown by the higher magnification BSE image in Fig. 6c.

A FIB cross section for FE-STEM characterization was prepared from the area shown by the white line in Fig. 6a. The cross section encompasses a continuous layer of laser-altered material covering a single olivine grain that borders a surface depression (see Fig. 6a). FE-STEM bright-field (BF) imaging shows that the altered layer is similar in thickness to what has been observed in laser-irradiated plagioclase grains (Moroz et al. 2014). Specifically the altered layer is thickest (0.8–1.0 μm) on the side of the grain that slopes down into the depression, then progressively tapers to a thickness of <0.5 μm over the top or "crest" of the grain away from depression. The images also show that in the thickest part of the altered region, there are three microstructurally distinct layers. EDX shows that each of these layers are composed of silicate glass with varying modal fractions of $npFe^0$ spherules and/or nanocrystalline silicate material (Figs. 7a and 7b). In addition, clusters of larger $npFe^0$ spherules 100–300 nm diameter occur locally within the altered layer, consistent with our SEM observations (Fig. 6). The first sublayer, which forms the immediate surface of the altered grain, is 50–300 nm wide and composed of approximately 40–50 modal% $npFe^0$ spherules 5–20 nm in size (Figs. 7a and 7b).

Underneath sublayer 1 is a glass layer (sublayer 2; Fig. 7), which has a much lower modal concentration of $npFe^0$ (<0.5%) relative to sublayer 1 and contains scattered nanoscale regions with short range crystalline order identifiable in high-resolution TEM images. The third sublayer in the sequence, at the bottom of the altered region, is between 200 and 400 nm thick and is composed predominantly of more irregularly shaped nanocrystalline grains that are 10–50 nm in size (Fig. 7a). In portions of this layer, the grains are intergrown along shared grain boundaries with little or no surrounding glass, while in other areas they are isolated within a glassy matrix. The d-spacings of both individual reflections and ring patterns in selected-area electron diffraction patterns of the aggregates suggest most of these grains are olivine, with a subordinate amount of $npFe^0$.

In quantified EDX element maps, the elemental wt% of Fe in the topmost sublayer (sublayer 1) was enhanced by a factor of 2.5 higher relative to the wt% Fe in the underlying olivine grain, while Mg and Si were depleted by 20% and 10% respectively. Sublayers 2 and 3 both show trends in Fe and Mg that are opposite to sublayer 1: Fe is depleted by 80–90% and Mg is enriched by 20–30% relative to the underlying

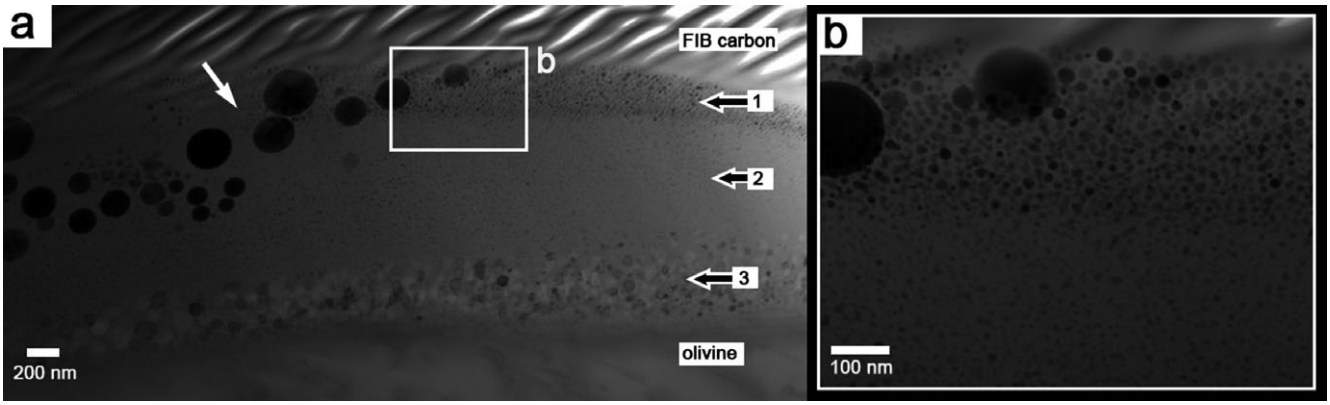

Fig. 7. Bright-field FE-STEM images of a FIB section extracted from the laser-altered material on the sloping side of an olivine single crystal taken from the 99-pulse Fo_{90}-pressed pellet sample. a) Sequence of three microstructurally distinct sublayers (numbered arrows) found in the laser-altered material (see text). White arrow indicates a cluster of larger diameter (50–200 nm) nanophase metallic Fe spherules (dark ovoid objects). b) Bright-field FE-STEM image of inset outlined in (a) showing a high concentration of 5–20 nm diameter nanophase metallic Fe spherules in uppermost layer 1 on surface of the laser-altered region.

olivine. Si is, however, depleted in sublayers 2 and 3 in much the same manner as in sublayer 1.

DISCUSSION

Brief Overview of Laser Ablation of Insulators

It is well known that the surfaces of solid materials can be heavily modified by high-power pulsed-laser irradiation. The process by which surface material is removed (ablated) is highly dependent on the laser fluence (J cm^{-2}): at low fluences the material can leave through simple evaporation from the surface, while at higher fluences a plasma can be created in the ejected plume. Predicting the degree to which a laser will ablate any material is complicated, as the interaction will depend on a number of factors, such as the laser fluence, pulse width, wavelength, and absorption coefficient of the sample. For wide band-gap materials, such as the insulators studied here, although the absorptivity of the sample is low at the 193 nm wavelength used, the sample can still absorb light. This occurs through multiphoton absorption (Tsai et al. 1988; Shen et al. 1989), via defects initially present at the surface or subsequently created during irradiation (Ihlemann et al. 1992; Pedraza 1998). In multiphoton absorption, the electrons are excited into the conduction band of the solid by absorbing more than one photon, whereby they can absorb light at any wavelength, subsequently transferring energy in the solid. Defects are present in all materials to some degree and break the periodicity of the lattice structure, creating absorption states in the band gap that can absorb light. Regardless of how the light is absorbed, the damage can produce more defects and changes in surface structure that can further enhance a sample's efficiency to absorb light. Furthermore, the absorption of high intensity light and ablation efficiency of transparent material has also been shown to increase with the surface roughness (Ihlemann et al. 1992), potentially as a result of avalanche ionization (Bloembergen 1974), where the increased electric fields on the rough surfaces produce dielectric breakdown, creating a plasma that renders the material opaque. Thus, although the materials studied here have band gaps >8 eV (Nitsan and Shankland 1976), larger than the laser photon energy in our experiments, we expected that both olivine and SiO_2 would be ablated at some level by our laser.

Factors in Comparing Laser Irradiation Effects in Different Minerals

For the current set of measurements, as in previous space weathering experiments (Loeffler et al. 2008, 2009), we studied samples that were similar in composition, Fo_{90} and Fo_{99+}, to investigate how irradiation effects varied in samples that had different intrinsic Fe contents. However, comparing sample-to-sample effects in the ion irradiation experiments on the basis of fluence is subject to fewer uncertainties than these laser experiments, where the amount of light absorbed during each pulse and how it is absorbed may vary with mineral composition, as the material optical properties change.

Reddening and Darkening in SiO_2

Of the three samples, the spectral changes resulting from laser irradiation of the SiO_2 sample are the least prominent (Fig. 3). After 49 pulses, the reddening is ~10

times less for SiO_2 than olivine samples and the change in reflectance at 2 μm is more than five times lower and in the other direction (the sample brightens).

Spectral reddening in the SiO_2 sample is not evident until after the seventh laser pulse (Fig. 3), when the spectral slope begins to increase slowly with fluence. This threshold is similar to what has been reported for ablation studies on crystalline and amorphous SiO_2 (Ihlemann 1992; Pedraza 1998), which show similar fluence thresholds for the onset of ablation. This behavior has been attributed to the buildup of defects in the sample, which increase the sample's absorptivity; the absorption for SiO_2 has been modeled to be extremely low at 193 nm (Awazu 2004). Once the threshold has been reached, the sample ablates at a nearly linear rate (Ihlemann et al. 1992; Pedraza 1998). We note that the threshold we observe is slightly lower than in previous studies. However, we speculate this can still explain why little to no spectral change is observed for a low number of laser pulses, as the threshold appears to be highly dependent on a number of factors, such as sample surface roughness (Ihlemann et al. 1992), the phase of the SiO_2 (Pedraza 1998), and laser wavelength (Awazu 2004). Once the ablation threshold is reached in our samples the spectral slope increases linearly with increased irradiation until the end of the experiment. The reddening observed can be explained by the formation of SiO_x, where $x < 2$ (Philipp 1971), which absorb strongly in the UV. We note that the formation of SiO and $SiO_{1.5}$ in laser-irradiated samples of SiO_2 has been reported previously, using XPS (Awazu 2004) and is consistent with the broadening of the Si-2p peak in our Fo_{90} and Fo_{99+} samples that were measured with XPS.

In addition to reddening, the SiO_2 brightens at 2 μm during irradiation. Half of the brightening (~3%) occurs after the first laser pulse, which is likely due to the removal of the adventitious carbon layer on the surface grains or simply a minor change in the macroscopic structure of the pressed pellet, i.e., some of the weakly bound grains may have fallen off of the sample. Similar to the case of reddening, no spectral changes occur until after seven pulses, whereby there is a slow increase in the reflectance at 2 μm. By the end of the experiment, the reflectance at 2 μm is about 3% higher than it was after seven laser pulses. We suspect that this small change is due to changes in sample topography, such as surface melting/smoothing of the surface. We note that previous experiments showed that ablating Fo_{99+} onto unirradiated Fo_{99+} powders caused significant topography changes (see fig. 9 in Loeffler et al. 2008) and brightened the powders by ~4%. A similar conclusion was made by Moroz et al. (2014), who observed brightening in plagioclase pellets that had been laser irradiated. We point out that brightening has also been reported for dark minerals that have been ion irradiated, although the process may be different (Vernazza et al. 2013), as the initial reflectance is much lower.

Reddening and Darkening in Fo_{90} and Fo_{99+}

Previous laboratory measurements have shown that the absorption of Fo_{90} and Fo_{99+} at 193 nm are comparable (Nitsan and Shankland 1976), and thus in the following discussion we consider that the absorbed laser fluence for these two olivine samples is similar. This is consistent with our earlier studies that showed the ablation rate for these two minerals was similar (Loeffler et al. 2008).

Spectral reddening and darkening occur during laser irradiation for both Fo_{90} and Fo_{99+} pellet samples. For the Fo_{90} sample, the reddening occurs quickly and irradiation beyond ~13 pulses does not additionally increase the spectral slope of the olivine, yet the fraction of metallic Fe continues to increase (Fig. 8). The lack of correlation between the metallic fraction and spectral reddening is different from our previous ion irradiation experiments, plotted for comparison in Fig. 8, which showed that these two parameters were correlated (Loeffler et al. 2009). We suspect that the difference observed here is that, while repeated laser pulses increase the Fe^0/Fe on the surface, they also heat the sample, allowing the metallic Fe grains to undergo microstructural coarsening (e.g., Ostwald ripening), increasing the size of the iron nanoparticles. The larger particles do not contribute to the reddening but are more effective at darkening the sample (Noble et al. 2007). This hypothesis is also supported by our FE-SEM and FE-STEM observations, which show a small number of larger (100–200 nm) $npFe^0$ grains that are likely growing at the expense of the smaller (<50 nm) grains.

During laser irradiation, the spectral changes observed in the Fo_{99+} pellet sample are initially less than in the Fo_{90} sample, which is consistent with the hypothesis that reddening and darkening are being caused by the production of reduced Fe nanoparticles from the precipitation of Fe present in low concentration in the sample. Given that spectral reddening has been correlated with small $npFe^0$ (Noble et al. 2007), the observation that the Fo_{99+} sample continues to redden up to the point where it is similar in magnitude to the Fo_{90} (Fig. 3) sample suggests that after a large number of laser pulses the small $npFe^0$ present in each sample may be similar. Consequently, the number of large Fe precipitates would have to be much smaller in the Fo_{99+} sample, given the significantly lower concentration of Fe, which is reasonable considering that the Fo_{99+} sample does not

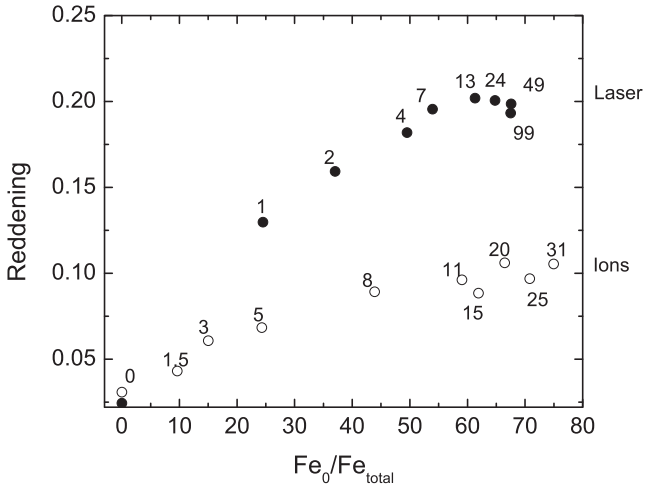

Fig. 8. Comparison of the reddening in the Fo_{90} sample to the formation of metallic Fe, as indicated by XPS for both laser (this work) and ion (Loeffler et al. 2009) irradiation. The numbers beside the points correspond to the number of pulses (laser) and the ion fluence (ions, in units of 10^{17} ions cm^{-2}).

begin to darken until after 13 laser pulses. It is at this point that the rate of spectral reddening decreases, suggesting that some of the smaller grains precipitated into larger $npFe^0$ particles. Future studies with the electron microscope could confirm this hypothesis.

It is interesting to note that the different weathering rates for our two olivine samples are also consistent with recent laboratory studies (Moroz et al. 2014) on the laser irradiation of natural plagioclase (An_{47-52}), which contained an intermediate Fe concentration (0.72 wt% FeO). In those experiments, one laser pulse caused the spectral slope to increase two times more than it increased after a single shot in our Fo_{99+} sample and about two times less than it increased after a single shot in our Fo_{90} sample. Subsequent irradiation of Moroz et al.'s plagioclase sample further increased the spectral slope, suggesting that similar trends as those quantified in our experiments (Fig. 3) would be observed in those experiments with successive irradiation. More detailed comparison between these studies, as well as others, is desired, but is not currently possible given the differences in the experimental conditions, such as laser wavelength and fluence, as well as the likelihood that the mineral composition and structure also affect its susceptibility to weathering (Yamada et al. 1999; Brunetto et al. 2006a; Moroz et al. 2014).

Comparison to Other Experiments on Fo_{90}

In Fig. 9, we compare these laser irradiation experiments with other irradiation experiments on Fo_{90}. To focus on the spectral changes observed in the experiments, we divided the spectrum of the irradiated olivine sample by that of the unirradiated olivine sample. We note that this is a qualitative comparison as the scattering properties of the sample depend on both the grain size and phase angle, and these are slightly different for the different studies. Figure 9 (top) compares experiments where Fo_{90} was irradiated with a ns-pulsed laser (this study), irradiated with 4 keV He^+ ions (Loeffler et al. 2009), and coated with vapor produced from irradiating another olivine sample (Loeffler et al. 2008), while Fig. 9 (bottom) compares the reflectance spectra of Fo_{90} taken after a single laser pulse. It is clear from these experiments that regardless of the irradiation approach, the shape of the weathered spectra are similar, which suggests that in all cases these changes are likely caused by the chemical reduction of Fe through the formation of $npFe^0$. Furthermore, judging from Fig. 9 (bottom), the spectral change was the largest when the sample was irradiated at the highest laser fluence.

Metallic Fe Formation in Fo_{90}

Much of work investigating how the metallic Fe is created during irradiation has been performed previously by Hapke and coworkers (see Hapke [2001] and references therein). The main conclusion from these studies is that the metallic Fe is only formed when material is sputtered from the surface and redeposited, as opposed to being directly produced by irradiation. Later experiments using the laser to evaporate Fo_{90} confirmed with chemical analysis that the evaporated deposits do indeed contain metallic Fe (Loeffler et al. 2008). However, using similar in situ techniques it was also found that metallic Fe was formed when sectioned rocks of olivine, where redeposition is assumed to be negligible, were irradiated with He ions (Dukes et al. 1999; Davoisne et al. 2008; Loeffler et al. 2009), suggesting that direct irradiation can also produce metallic Fe. This debate has also been extended to the spectral changes occurring as a result of laser irradiation (e.g., Sasaki et al. 2001). Thus, we also irradiated multiple flat Fo_{90} sections. In all cases, XPS spectra showed that the Fe in the rock reduced to Fe^0 at a faster rate than in the powdered sample, and in some cases the metallic Fe on the surface reached equilibrium after a single laser pulse. The difference between the rock and the powder could be due to a significant percentage of the redeposited material being oxidized, as was observed previously (Loeffler et al. 2008). Yet, given the discussion above regarding how the laser ablation of insulators are strongly affected by the sample roughness (Ihlemann et al. 1992), this conclusion is less definitive than in the case of ion irradiation.

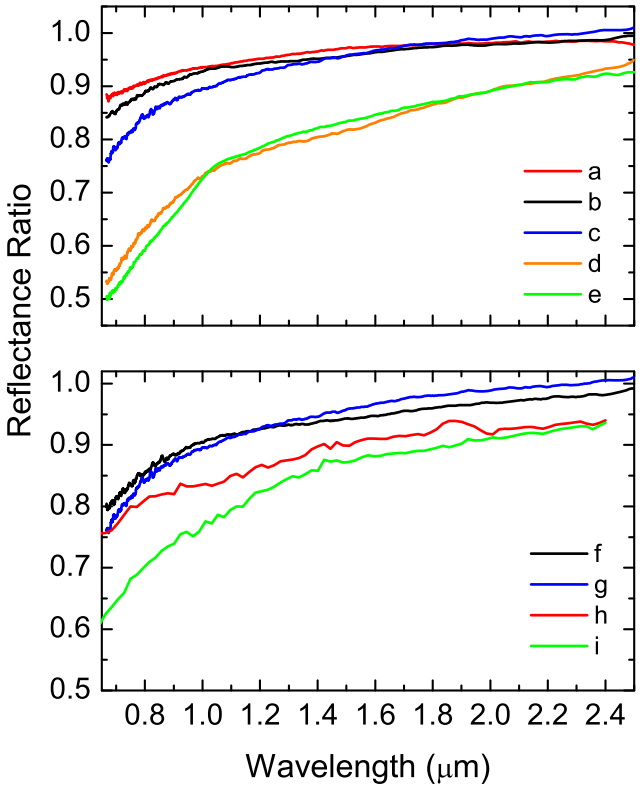

Fig. 9. The reflectance spectra of an altered Fo_{90}-pressed pellet divided by the unaltered sample. Top (from top to bottom at 700 nm) a) after ablating 175 nm of Fo_{90} onto a fresh sample (Loeffler et al. 2008), b) after irradiation with 2.5×10^{18} 4 keV He^{+} cm^{-2} (Loeffler et al. 2009), c) after one laser pulse (this work), d) after 25 laser pulses (this work), and e) after ablating 1338 nm of Fo_{90} onto a fresh Fo_{90} sample (Loeffler et al. 2008). Bottom (from top to bottom at 1 μm): samples after one laser pulse: f) <45 μm grain size fraction (this work), g) 45–125 μm (this work), h) <80 μm, 12 J cm^{-2} (Sasaki et al. 2001), i) <80 μm, 24 J cm^{-2} (Sasaki et al. 2001).

Implications for Natural Space Weathering

The implications of the current experimental results for natural space weathering depend to varying degrees on how well the experiments simulate the processes and products of natural small-scale (e.g., micrometeorite) hypervelocity impacts. Previous studies have used energetic comparisons between laser irradiations and micrometeorite impacts to estimate regolith impact-exposure ages based on laser irradiation experiments (Sasaki et al. 2001; Loeffler et al. 2009). Although the current results could conceivably refine such estimates, the energy comparison approach remains hampered by fundamental unknowns, such as the efficiency at which impact kinetic energy is converted into thermal energy or the relative importance that the momentum transferred from the impactor may play in altering the surface. The problem is compounded by additional lack of knowledge concerning how impact-generated thermal energy itself is converted into a given amount of shock melt and $npFe^0$, especially when mechanical shock adds to the process. Once these aspects of the hypervelocity impact process become well quantified through theory and experiment, a better basis of extrapolation between laser irradiation results and natural hypervelocity impacts should be possible.

The optical reflectance results, at least for the Fo_{90} olivine pellet sample, suggest the samples are good spectral analogs for natural space weathered regoliths of similar mineralogical composition, such as ordinary chondrite parent materials on S-type asteroids. Finding naturally space weathered samples of similar mineralogical composition to the Fo_{90} olivine pellet for microscopic analysis, such as those in olivine-rich meteorite/asteroidal regolith breccias or the Hayabusa samples, has been difficult (Noble et al. 2010; Keller et al. 2013; Noguchi et al. 2014; Thompson et al. 2014). Lunar soils, which have been studied extensively by microscopic analysis, are typically dominated by minerals other than olivine, and thus are harder to compare. However, we point out that the laser-irradiated Fo_{90} samples studied here appear to be similar in their $npFe^0$ microstructure to impact vapor and agglutinitic melt deposits in mature lunar soils (e.g., Keller and Clemett 2001; Keller and McKay 1997). For instance, microscope analysis shows that sublayers 1–3 are amorphous, indicating that these regions have either been melted or evaporated and redeposited during laser irradiation. Sublayer one is likely a vapor deposit, as the enrichment of Fe and high modal concentration of $npFe^0$ <20 nm size present is consistent for what has been found in vapor deposits on lunar regolith grains (Keller and McKay 1997; Keller and Clemett 2001). Sublayer 2 and 3 are likely melt deposits, as they are chemically similar to the bulk grain but lack the fine-grained $npFe^0$ found in sublayer 1 characteristic of vapor deposits. The nanocrystalline olivine found in sublayer 3, adjacent to the olivine substrate, also likely crystallized from the melt formed by the laser, possibly promoted by local thermal gradients or heterogenous nucleation on the underlying olivine.

Assuming there is sufficient basis to use the current Fo_{90} and Fo_{99+} sample results as an analog for impact-generated asteroid space weathering, a few implications can be drawn. The step-wise experimental approach of this study, in which optical reflectance was tracked as a function of increasing laser fluence, has produced data supporting the concept that as asteroid regoliths accumulate melt and vapor deposits from micrometeorite impact, their optical properties should reach a steady state or "saturation." This saturation would necessarily be tied to the amount of $npFe^0$ produced in the deposits

as a function of accumulated micrometeorite impacts over time, an amount that may be much smaller compared to lunar samples (Noble et al. 2010; Keller et al. 2013; Noguchi et al. 2014; Thompson et al. 2014). Alternatively, however, other optically active nanoscale grains such as Fe-sulfides could substitute, in their optical effects, for the $npFe^0$ (Keller et al. 2013). In either case, the current results suggest that optical reddening, which is correlated with $npFe^0$ grains less than ~10–20 nm in size (Noble et al. 2007), could be expected to reach saturation at an earlier stage in regolith evolution compared to darkening (Fig. 3). This saturation would be achieved when the volume fraction of sub-20 nm $npFe^0$ in the regolith became similar to that of the Fo_{90} pellet sample after 10 laser pulses (this volume fraction was not measured by TEM or other methods in this study). Darkening, on the other hand, would not reach steady state until the volume fraction of larger (>40 nm) $npFe^0$ grains became similar to the value of approximately 0.5 vol% we estimated for the 99 pulse Fo_{90} pellet sample. Assuming a steady-state micrometeorite flux, with no resurfacing from major impacts, the time needed to reach steady state in the case of either reddening or darkening would necessarily take longer if the olivine had less Fe than the Fo_{90} composition. Whether it would be accelerated for compositions more Fe-rich than Fo_{90} cannot be determined based on our experiments, but has been discussed by Moroz et al. (2014).

CONCLUSIONS

Pulsed-laser irradiation, used to simulate micrometeorite impacts, can alter the reflectance spectrum of Fe-bearing and non-Fe-bearing minerals. For Fo_{90} and Fo_{99+} olivine samples, the irradiation causes the spectral slope to redden and the overall reflectance to decrease. In addition, irradiation causes the band area of the 1 μm absorption band, observable in the Fo_{90} samples, to decrease slightly during irradiation, with no shift in peak position. Laser irradiation of SiO_2 results in a reddened spectral slope similar to that of the olivine sample and brightening after an incubation dose. The spectral reddening observed from the ultraviolet to the near-infrared is consistent with the formation of SiO or other SiO_x species, which absorb light in this region. The low degree of brightening is consistent with a change in the surface topography of the sample, which has been observed previously. The observation that the near-infrared spectra of non-Fe-bearing minerals can also be altered via irradiation suggests that other minerals may also contribute to spectral change due to space weathering observed via remote sensing.

In situ surface chemical analysis of the Fo_{90} samples shows that the majority of Fe present on the mineral surface reduces to a metallic state. However, this reduction does not correlate with spectral reddening, as it had in previous ion irradiation studies, as the sample stops reddening while $npFe^0$ continues to increase with further laser irradiation. However, the chemical reduction of Fe does correlate fairly well with the spectral changes if we include both darkening and reddening. This difference, as compared to our previous ion irradiation studies, is reasonable as while successive laser pulses create new small $npFe^0$ particles, they also catalyze the aggregation of small $npFe^0$ into larger $npFe^0$, involved in darkening. This hypothesis is supported by the observation that the sample continues to darken after the reddening reaches equilibrium and by our electron microscope studies, which show the presence of both small (20–50 nm) and large (100–400 nm) $npFe^0$ in the irradiated sample.

Extrapolating our results to airless bodies, the sequence of spectral alteration observed in our Fo_{90} samples, in which end-state or "saturated" optical reddening precedes end-state darkening as laser deposits accumulate, suggests a similar relative sequence may occur on asteroid bodies with regoliths dominated by olivine. The sequence would be tied to differences in formation efficiency, optical absorption efficiency or both, for smaller $npFe^0$ (<40 nm) associated with vapor-dominated deposition that promote reddening, as opposed to larger $npFe^0$ (>40 nm) responsible for darkening.

Acknowledgments—This work was supported by the NASA Cosmochemistry, Lunar Advanced Science and Exploration Research, and Solar System Workings programs, as well as NSF's Astronomy and Astrophysics Research Grants program (C.D. and R.B.). The authors would like to thank Lindsay Keller for his comments on the manuscript.

Editorial Handling—Dr. Carle Pieters

REFERENCES

Adams J. and McCord T. 1971. Optical properties of mineral separates, glass, and anorthositic fragments from Apollo mare samples. 2nd Lunar Science Conference 3: pp. 2183–2195.

Awazu K. 2004. Ablation and compaction of amorphous SiO_2 irradiated with ArF excimer laser. *Journal of Non-Crystalline Solids* 337:241–253.

Balberg I. and Pinch H. L. 1978. The optical absorption of iron oxides. *Journal of Magnetism and Magnetic Materials* 7:12–15.

Bloembergen N. 1974. Laser-induced electric breakdown in solids. *IEEE Journal of Quantum Electronics* 10:375–386.

Brunetto R., Romano F., Blanco A., Fonti S., Martino M., Orofino V., and Verrienti C. 2006a. Space weathering of silicates simulated by nanosecond pulse UV excimer laser. *Icarus* 180:546–554.

Brunetto R., Vernazza P., Marchi S., Birlan M., Fulchignoni M., Orofino V., and Strazzulla G. 2006b. Modeling asteroid surfaces from observations and irradiation experiments: The case of 832 Karin. *Icarus* 184:327–337.

Burns R. G. 1993. *Mineralogical applications of crystal field theory*. New York: Cambridge University Press.

Chapman C. R. 2004. Space weathering of asteroid surfaces. *Annual Review of Earth and Planetary Sciences* 32:539–567.

Cintala M. J. 1992. Impact-induced thermal effects in the lunar and mercurian regoliths. *Journal of Geophysical Research-Planets* 97:947–973.

Clark B. E. and Fanale F. P. 1992. Meteorite-asteroid sectral comparison: The effects of comminution, melting and recrystallization. *Icarus* 97:288–297.

Clark B. E., Hapke B. W., Pieters C. M., and Brit D. 2002. Asteroid space weathering and regolith evolution. In *Asteroids III*, edited by Bottke W. F. Tucson, Arizona: The University of Arizona Press. pp. 585–599.

Cliff G. and Lorimer G. A. 1975. The quantitative analysis of thin specimens. *Journal of Microscopy* 103:203–207.

Davoisne C., Leroux H., Frere M., Gimblot J., Gengembre L., Djouadi Z., Ferreiro V., d'Hendecourt L., and Jones A. 2008. Chemical and morphological evolution of a silicate surface under low-energy ion irradiation. *Astronomy & Astrophysics* 482:541–548.

Dukes C. A., Baragiola R. A., and McFadden L. A. 1999. Surface modification of olivine by H^+ and He^+ bombardment. *Journal of Geophysical Research-Planets* 104:1865–1872.

Gaffey M. J. 2010. Space weathering and the interpretation of asteroid reflectance spectra. *Icarus* 209:564–574.

Gaffey M. J., Bell J. F., Hamilton Brown R., Burbine T. H., Piatek J. L., Reed K. L., and Chaky D. A. 1993. Mineralogical variations within the S-type asteroid class. *Icarus* 106:573–602.

Hapke B. 1973. Darkening of silicate rock powders by solar wind sputtering. *Moon* 7:342–355.

Hapke B. 2001. Space weathering from Mercury to the asteroid belt. *Journal of Geophysical Research—Planets* 106:10,039–10,073.

Hapke B., Cassidy W., and Wells E. 1975. Effects of the vapor-phase deposition processes on the optical, chemical, and magnetic properties of the lunar regolith. *Moon* 13:339–353.

Hendrix A. and Vilas F. 2006. The effects of space weathering at UV wavlengths: S-class asteroids. *The Astronomical Journal* 132:1396–1404.

Hochella M. F. J. and Brown G. E. J. 1988. Aspects of silicate surface and bulk structure analysis using x-ray photoelectron spectroscopy. 8th Lunar Science Conference 3: pp. 1641–1648.

Housley R. and Grant R. 1977. An XPS (ESCA) study of the lunar surface alteration profiles. *Geochimica et Cosmochimica Acta* 8:3885–3889.

Ihlemann J. 1992. Excimer laser ablation of fused silica. *Applied Surface Science* 54:193–200.

Ihlemann J., Wolff B., and Simon P. 1992. Nanosecond and femtosecond excimer laser ablation of fused silica. *Applied Physics A* 54:363–368.

Keller L. P. and McKay D. S. 1993. Discovery of vapor deposits in the lunar regolith. *Science* 261:1305–1307.

Keller L. P. and McKay D. S. 1994. The nature of agglutinitic glass in the fine-size fraction of lunar soil 10084. Proceedings, 25th Lunar and Planetary Science Conference. pp. 658–686.

Keller L. P. and Clemett S. J. 2001. Formation of nanophase Fe in the lunar regolith (abstract #2097). 32nd Lunar and Planetary Science Conference. CD-ROM.

Keller L. P. and McKay D. S. 1997. The nature and origin of rims on lunar soil grains. *Geochimica et Cosmochimica Acta* 61:2331–2341.

Keller L. P., Rahman Z., Hiroi T., Sasaki S., Noble S. K., Horz F., and Cintala M. J. 2013. Asteroidal space weathering: The major role of FeS (abstract #2404). 44th Lunar and Planetary Science Conference. CD-ROM.

Kissel J. and Krueger F. R. 1987. Ion formation by impact of fast dust particles and comparison with related techniques. *Applied Physics A* 42:69–85.

Loeffler M. J., Baragiola R. A., and Murayama M. 2008. Laboratory simulations of redeposition of impact ejecta on mineral surfaces. *Icarus* 196:285–292.

Loeffler M. J., Dukes C. A., and Baragiola R. A. 2009. Irradiation of olivine by 4 keV He+: Simulation of space weathering by the solar wind. *Journal of Geophysical Research—Planets* 114:3003.

Moroz L. V., Fisenko A. V., Semjonova L. F., Pieters C. M., and Korotaeva N. N. 1996. Optical effects of regolith processes on S-asteroids as simulated by laser shots on ordinary chondrite and other mafic materials. *Icarus* 122:366–382.

Moroz L. V., Starukhina L. V., Rout S. S., Sasaki S., Helbert J., Baither D., Bischoff A., and Hiesinger H. 2014. Space weathering of silicate regoliths with various FeO contents: New insights from laser irradiation experiments and theoretical spectral simulations. *Icarus* 235:187–206.

Nash D. B. 1967. Proton-irradiation darkening of rock powders—Contamination and temperature effects and applications to solar-wind darkening of Moon. *Journal of Geophysical Research* 72:3089–3104.

Nash D. B. and Conel J. E. 1973. Vitrification darkening of rock powders: Implications for the optical properties of the lunar surface. *Moon* 8:346–364.

Nitsan U. and Shankland T. J. 1976. Optical properties and electronic structure of mantle silicates. *Geophysical Journal of the Royal Astronomical Society* 45:59–87.

Noble S. K., Pieters C. M., and Keller L. P. 2007. An experimental approach to understanding the optical effects of space weathering. *Icarus* 192:629–642.

Noble S. K., Keller L. P., and Pieters C. M. 2010. Evidence of space weathering in regolith breccias II: Asteroidal regolith breccias. *Meteoritics & Planetary Science* 45:2007–2015.

Noble S. K., Hiroi T., Keller L. P., Rahman Z., Sasaki S., and Pieters C. M. 2011. Experimental space weathering of ordinary chondrites by nanopulse laser: TEM results (abstract #1608). 42nd Lunar and Planetary Science Conference. CD-ROM.

Noguchi T., Kimura M., Hashimoto T., Konno M., Nakamura T., Zolensky M. E., Okazaki R., Tanaka M., Tsuchiyama A., Nakato A., Ogami T., Ishida H., Sagae R., Tsujimoto S., Matsumoto T., Matsuno J., Fujimura A., Abe M., Yada T., Mukai T., Ueno M., Okada T., Shirai K., and Ishibashi Y. 2014. Space weathered rims

found on the surfaces of the Itokawa dust particles. *Meteoritics & Planetary Science* 49:188–214.

Pedraza A. J. 1998. Interaction of UV laser light with wide band gap materials: Mechanisms and effects. *Nuclear Instruments and Methods in Physics Research Section B* 141:709–718.

Philipp H. R. 1966. Optical transitions in crystalline and fused quartz. *Solid State Communications* 4:73–75.

Philipp H. R. 1971. Optical properties of non-crystalline Si, SiO, SiOx, and SiO_2. *Journal of Physical Chemistry Solids* 32:1935–1945.

Pieters C. M., Fischer E. M., Rode O., and Basu A. 1993. Optical effects of space weathering: The role of the finest fraction. *Journal of Geophysical Research* 98:20817–20824.

Sanchez J. A., Reddy V., Kelley M. S., Cloutis E. A., Bottke W. F., Nesvorný D., Lucas M. P., Hardersen P. S., Gaffey M. J., Abell P. A., and Corre L. L. 2014. Olivine-dominated asteroids: Mineralogy and origin. *Icarus* 228:288–300.

Sasaki S., Nakamura K., Hamabe Y., Kurahashi E., and Hiroi T. 2001. Production of iron nanoparticles by laser irradiation in a simulation of lunar-like space weathering. *Nature* 410:555–557.

Sasaki S., Kurahashi E., Yamanaka C., and Nakamura K. 2003. Laboratory simulation of space weathering: Changes of optical properties and TEM/ESR confirmation of nanophase metallic iron. *Advances in Space Research* 31:2537–2542.

Schott J. and Berner R. A. 1983. X-ray photoelectron studies of the mechanism of iron silicate dissolution during weathering. *Geochimica et Cosmochimica Acta* 47:2233–2240.

Seah M. P. and Dench W. A. 1979. Quantitative electron spectroscopy of surfaces: A standard data base for electron inelastic mean free path in solids. *Surface and Interface Analysis* 1:2–11.

Shankland T. J. 1968. Band gap of forsterite. *Science* 161:51–53.

Shen X. A., Jones S. C., and Braunlich P. 1989. Laser-heating of free-electrons in wide-gap optical-materials at 1064 nm. *Physical Review Letters* 62:2711–2713.

Smith D. and Adams N. G. 1973. Studies of plasma production at hypervelocity microparticle impact. *Journal of Physics D Applied Physics* 6:700–719.

Strazzulla G., Dotto E., Binzel R., Brunetto R., Barucci M. A., Blanco A., and Orofino V. 2005. Spectral alteration of the meteorite Épinal (H5) induced by heavy ion irradiation: A simulation of space weathering effects on near-Earth asteroids. *Icarus* 174:31–35.

Sugita S., Kadono T., Ohno S., Hamano K., and Matsui T. 2003. Does laser ablation vapor simulate impact vapor? (abstract #1573). 34th Lunar and Planetary Science Conference. CD-ROM.

Thompson M. S., Christoffersen R., Zega T. J., and Keller L. P. 2014. Microchemical and structural evidence for space weathering in soils from asteroid Itokawa. *Earth, Planets and Space* 66:Article 89.

Tsai T. E., Griscom D. L., and Friebele E. J. 1988. Mechanism of intrinsic Si E'-center photogeneration in high-purity silica. *Physical Review Letters* 61:444–446.

Vernazza P., Fulvio D., Brunetto R., Emery J. P., Dukes C. A., Cipriani F., Witasse O., Schaible M. J., Zanda B., Strazzulla G., and Baragiola R. A. 2013. Paucity of Tagish Lake-like parent bodies in the asteroid belt and among Jupiter Trojans. *Icarus* 225:517–525.

Yamada M., Sasaki S., Nagahara H., Fujiwara A., Hasegawa S., Yano H., Hiroi T., Ohashi H., and Otake H. 1999. Simulation of space weathering of planet-forming materials: Nanosecond pulse laser irradiation and proton implantation on olivine and pyroxene samples. *Earth, Planets and Space* 51:1255–1265.

Yin L. I., Ghose S., and Adler I. 1971. Core binding energy difference between bridging and nonbridging oxygen atoms in a silicate chain. *Science* 173:633–635.

Yin L. I., Tsang T., and Adler I. 1975. Electron spectroscopic studies related to solar-wind darkening of lunar-surface. *Geophysical Research Letters* 2:33–36.